



NEW

AX / AX R

Confocal Microscope Systems

Capture More Data in Less Time

- Gentler, faster, more sensitive imaging
- Resonant scanning with 2K pixel resolution for uncovering incredible details at high-speed
- See more of your sample with the world's largest field of view
- Fully integrated AI tools for simpler acquisition and more efficient data extraction.




www.microscope.healthcare.nikon.com/ax

 [nikon-instruments-inc-](https://www.linkedin.com/company/nikon-instruments-inc)

 [nikoninstrumentsinc](https://www.facebook.com/nikoninstrumentsinc)



 [nikoninst](https://twitter.com/nikoninst)

 [nikoninstruments](https://www.instagram.com/nikoninstruments)

Nikon Instruments Inc. • www.microscope.healthcare.nikon.com • nikoninstruments.us@nikon.com

RESEARCH ARTICLE

Puromycin-sensitive aminopeptidase is required for C2C12 myoblast proliferation and differentiation

Shion Osana¹  | Yasuo Kitajima^{2,3} | Naoki Suzuki⁴ | Aki Nunomiya⁵ | Hiroaki Takada⁶ | Takahiro Kubota⁶ | Kazutaka Murayama⁷ | Ryoichi Nagatomi^{1,6} 

¹Division of Biomedical Engineering for Health and Welfare, Graduate School of Biomedical Engineering, Tohoku University, Sendai, Japan

²Division of Developmental Regulation, Institute of Molecular Embryology and Genetics, Kumamoto University, Kumamoto, Japan

³Department of Immunology, Graduate School of Biomedical and Health Sciences, Hiroshima University, Hiroshima, Japan

⁴Department of Neurology, Graduate School of Medicine, Tohoku University, Sendai, Japan

⁵IFOM, The FIRC Institute of Molecular Oncology, Milan, Italy

⁶Department of Medicine and Science in Sports and Exercise, Graduate School of Medicine, Tohoku University, Sendai, Japan

⁷Division of Biomedical Measurements and Diagnostics, Graduate School of Biomedical Engineering, Tohoku University, Sendai, Japan

Correspondence

Shion Osana and Ryoichi Nagatomi, Division of Biomedical Engineering for Health and Welfare, Graduate School of Biomedical Engineering, Tohoku University, Seiryomachi 2-1, Aoba-Ku, Sendai, Miyagi 980-8575, Japan. Email: shionosana@med.tohoku.ac.jp (S. O.) and nagatomi@med.tohoku.ac.jp (R. N.)

Funding information

Japan Society for the Promotion of Science, Grant/Award Numbers: 18H04080, 20K19478

Abstract

The ubiquitin-proteasome system is a major protein degradation pathway in the cell. Proteasomes produce several peptides that are rapidly degraded to free amino acids by intracellular aminopeptidases. Our previous studies reported that proteolysis via proteasomes and aminopeptidases is required for myoblast proliferation and differentiation. However, the role of intracellular aminopeptidases in myoblast proliferation and differentiation had not been clarified. In this study, we investigated the effects of puromycin-sensitive aminopeptidase (PSA) on C2C12 myoblast proliferation and differentiation by knocking down PSA. Aminopeptidase enzymatic activity was reduced in PSA-knockdown myoblasts. Knockdown of PSA induced impaired cell cycle progression in C2C12 myoblasts and accumulation of cells at the G2/M phase. Additionally, after the induction of myogenic differentiation in PSA-knockdown myoblasts, multinucleated circular-shaped myotubes with impaired cell polarity were frequently identified. Cell division cycle 42 (CDC42) knockdown in myoblasts resulted in a loss of cell polarity and the formation of multinucleated circular-shaped myotubes, which were similar to PSA-knockdown myoblasts. These data suggest that PSA is required for the proliferation of myoblasts in the growth phase and for the determination of cell polarity and elongation of myotubes in the differentiation phase.

KEYWORDS

cell polarity, myoblast fusion, myogenic differentiation, proteasome, puromycin-sensitive aminopeptidase

1 | INTRODUCTION

The maintenance of skeletal muscle depends largely on muscle stem cells, also known as satellite cells, which supply myoblasts required for regeneration and growth (Morgan & Partridge, 2003; Yin

et al., 2013). Upon activation after skeletal muscle damage, satellite cells proliferate as myoblasts. They fuse each other to form multinucleated myotubes that are integrated into the damaged segments of skeletal muscle tissue (Brack & Rando, 2012). Owing to its regenerative capacity, skeletal muscle is capable of recovering from

This is an open access article under the terms of the Creative Commons Attribution-NonCommercial-NoDerivs License, which permits use and distribution in any medium, provided the original work is properly cited, the use is non-commercial and no modifications or adaptations are made.

© 2020 The Authors. *Journal of Cellular Physiology* Published by Wiley Periodicals LLC

damages induced by mechanical overload frequently experienced in strength training and sports activity.

The ubiquitin-proteasome system is one of the major intracellular protein degradation pathways (Collins & Goldberg, 2017; Goldberg, 2003). We previously demonstrated that proteasomal dysfunction in skeletal muscle resulted in significant impairments of muscle growth and development (Kitajima et al., 2014). We further demonstrated that a satellite cell-specific defect in proteasomal function led to the loss of satellite cells, which critically compromised the regenerative capacity of skeletal muscle tissue after cardiotoxin-induced damage. Primary myoblasts derived from proteasome-defective mice exhibited significantly impaired proliferative and differentiation abilities (Kitajima et al., 2018). These studies suggest that proteasome function is essential for myogenesis and the maintenance of the skeletal muscle tissues. The mechanism responsible for the impairment in proliferation and differentiation may therefore be dependent on the downstream processes after protein degradation.

Proteasomes generate oligopeptides containing 2–20 amino acids in the cytoplasm through protein degradation (Hershko & Ciechanover, 1992, 1998); the majority of these peptides are further digested by aminopeptidases into free amino acids (Botbol & Scornik, 1983, 1997; Saric et al., 2004). A variety of aminopeptidases, which selectively hydrolyze an amino acid residue from the N-terminus of proteins and peptides, have been identified in human cells (Mucha et al., 2010). In our recent study, we reported that the inhibition of intracellular aminopeptidase by bestatin methyl ester (Bes-ME) impaired the proliferation and differentiation of C2C12 myoblasts (Osana, Murayama, et al., 2020). Bes-ME is known to have a wider spectrum of inhibitory actions across various aminopeptidases (Mucha et al., 2010). Among bestatin-sensitive aminopeptidases, puromycin-sensitive aminopeptidase (PSA), a member of the M1 metalloprotease family, is abundantly expressed in skeletal muscle tissue. It has wide substrate specificity for substrates, such as leucine, alanine, lysine, and methionine (Constam et al., 1995; Sengupta et al., 2006). To the best of our knowledge, however, the effects of PSA on myogenesis have yet to be reported. In this study, we specifically investigated whether PSA knockdown in proliferating or differentiating C2C12 myoblasts affects myogenesis.

2 | MATERIALS AND METHODS

2.1 | Cell culture

Mouse C2C12 myoblasts were cultured under standard conditions (37°C under a humidified atmosphere containing 5% CO₂) in high-glucose Dulbecco's Modified Eagle Medium (DMEM; FUJIFILM Wako Pure Chemical Corporation) supplemented with 10% fetal bovine serum (Thermo Fisher Scientific) and 100 mg/ml penicillin–streptomycin solution (Sigma-Aldrich Corporation). Myogenic differentiation was induced in DMEM supplemented with 2% calf serum (Thermo Fisher Scientific) and 100 mg/ml penicillin–streptomycin. Most myoblasts begin to fuse after 1 or 2 days and form mature myotubes by 5 days. MyoD and myogenin are marker proteins of myogenic differentiation.

MyHC is the motor protein of thick muscle filaments (Zammit, 2017). Cells were cultured in 6-, 12-, or 24-well plates. For cell counting, we prepared a 1:1 dilution of the cell suspension using 0.4% trypan blue solution (Nacalai Tesque). Cells were counted in four 1-mm² square areas using a hemocytometer to determine the average number of cells.

2.2 | RNA interference

Three small interfering RNA (siRNA) sequences targeting PSA and CDC42 were produced by Sigma-Aldrich. siRNA#1, siRNA#2, and siRNA#3 corresponded to nucleotides 844–864, 1082–1102, and 493–513 of the PSA open-reading frame, respectively. In addition, siRNA#1 and siRNA#2 corresponded to nucleotides 211–231 and 230–250 of the CDC42 open-reading frame, respectively. A scramble sequence of siRNA was used as negative control. For siRNA experiments, the cells in each well were transfected with 20 nM PSA, CDC42, or scramble siRNAs using Lipofectamine RNAiMAX transfection reagent (Invitrogen) following the manufacturer's instruction.

2.3 | Quantitative real-time polymerase chain reaction (qPCR)

Total RNA was extracted from cultured cells using an RNeasy Mini Kit (Qiagen) and then reverse-transcribed into cDNA using a QuantiTect Reverse Transcription Kit (Qiagen). Real-time qPCR was performed using a StepOnePlus PCR System with SYBR Green Master Mix (Thermo Fisher Scientific). The primer sequences for C2C12 were as follows: *PSA* forward, TGTGGAAGCTGAACAGGTAGAA; *PSA* reverse, GGAACCATC CACTGAGGACA; *Myomaker* forward, ATCGCTACCAAGAGGCGTT; *Myomaker* reverse, CACAGCACAGACAAACCAGG; *Minion* forward, GGACCACTCCCAGAGGAAGGA; *Minion* reverse, GGACCGACGCCTG GACTAAC; *GAPDH* forward, AACTTTGGCATTGTGGAAGG; *GAPDH* reverse, CACATTGGGGGTAGGAACAC; *Ribosomal protein S13 (RPS13)* forward, TGCTCCACCTAATTGGAAA; and *RPS13* reverse, CTTGTG CACACAACAGCATTT.

2.4 | Western blot analysis

Total protein lysate was harvested using RIPA lysis buffer (ATTO Corporation) from the cultured cells for immunoblotting analysis. We used the bicinchoninic acid assay to determine protein concentrations. Next, we extracted the protein fractions using a reducing sample buffer containing 7% β-mercaptoethanol, a protease inhibitor, and a phosphatase inhibitor (ATTO Corporation). Protein extracts (10–20 μg per lane) were separated on a 5%–20% gradient sodium dodecyl sulfate-polyacrylamide gel and subsequently transferred to a polyvinylidene fluoride (PVDF) membrane using the Trans-Blot Turbo System (Bio-Rad Laboratories, Inc.). The PVDF membrane was blocked with 3% bovine serum albumin (Sigma-Aldrich) in 1×Tris-buffered saline–1% Tween-20 (FUJIFILM Wako Pure Chemical Corporation) for 1 h at room temperature.

The PVDF membrane was incubated with a primary antibody for 1 h at room temperature or overnight at 4°C with continuous shaking. The primary antibodies and dilution factors were as follows: anti-PSA (1:1000; Santa Cruz Biotechnology), anti-myosin heavy chain (MyHC, 1:1000; Santa Cruz Biotechnology), anti-Myogenin (1:500; Santa Cruz

Biotechnology), anti-MyoD (1:500; Santa Cruz Biotechnology), anti-cyclin D1 (1:3000; Proteintech), anti-cyclin B1 (1:1000; Cell Signaling Technology, Inc.), anti-CDK4 (1:1000; Proteintech), anti-CDK6 (1:1000; Proteintech), anti-P21 (1:1000; Proteintech), anti-CDC42 (1:1000; Abcam), and anti-glyceraldehyde-3-phosphate dehydrogenase (GAPDH;

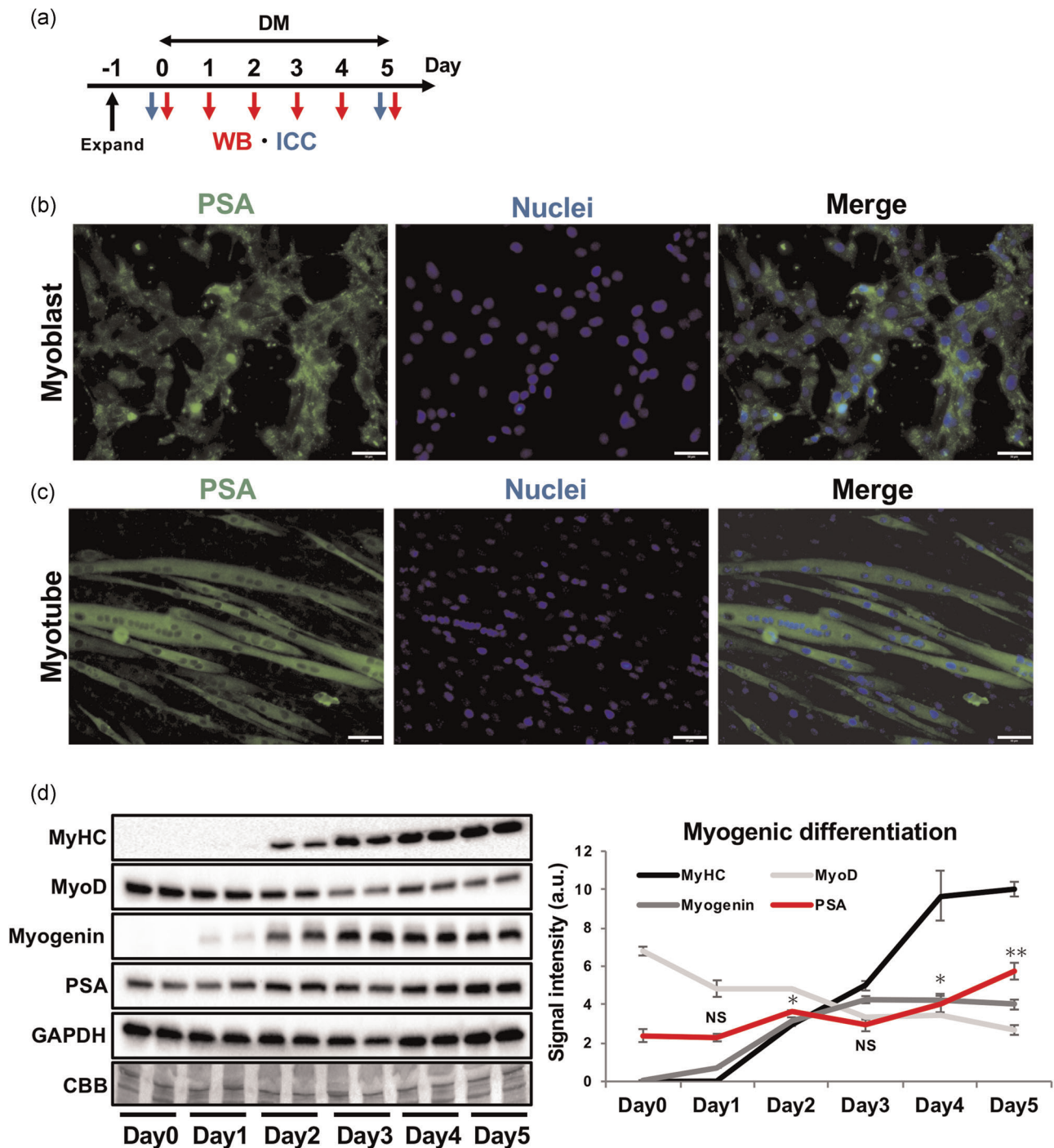


FIGURE 1 Localization and expression levels of PSA in C2C12 myoblasts and myotubes. (a) The time course of treatment and analysis. (b) Immunocytochemistry for PSA (green) and nuclei (blue) in myoblasts. PSA localized to the cytoplasm. Scale bar = 50 μ m. (c) Immunocytochemistry for PSA (green) and nuclei (blue) in myotubes. PSA localized to the cytoplasm. Scale bar = 50 μ m. (d) Immunoblotting of the protein levels of MyHC, myogenin, MyoD, and PSA during myogenic differentiation. The expression levels of MyHC and myogenin gradually increased during myogenic differentiation, whereas those of MyoD decreased. The expression level of PSA was significantly increased at 2, 4, and 5 days after the induction of myogenic differentiation. Values are presented as the mean \pm SEM (Student's *t*-test: NS, not significant, **p* < .05, ***p* < .01 vs. control; *n* = 4 per group). CBB, Coomassie brilliant blue; GAPDH, glyceraldehyde-3-phosphate dehydrogenase; MyHC, myosin heavy chain; MyoD, myoblast determination protein 1; PSA, puromycin-sensitive aminopeptidase

1:2000; Cell Signaling Technology). After repeated washing, the PVDF membrane was incubated in 2% nonfat milk containing a horseradish peroxidase-conjugated secondary antibody for 1 h. The resultant bands were visualized using enhanced chemiluminescence reagents (GE Healthcare). Finally, Coomassie brilliant blue (CBB; FUJIFILM Wako Pure Chemical Corporation) staining was performed following the manufacturer's instruction. In Western blot analysis, CBB-stained bands of 315 kDa were shown as the loading control. Densitometry was performed using Image Lab software (Bio-Rad Laboratories).

2.5 | Immunocytochemistry

Immunocytochemistry of C2C12 myoblasts and myotubes was performed as described previously (Osana, Kitajima, et al., 2020; Osana, Murayama, et al., 2020). Samples were incubated with

primary antibodies at 4°C overnight following blocking/permeabilization with phosphate-buffered saline containing 0.05% Triton X-100 and 5% goat serum for 60 min at room temperature. The immunocytochemistry of anti-PSA (1:100; Santa Cruz Biotechnology), anti-Ki67 (1:500; Abcam), anti-MyHC (1:200; Developmental Studies Hybridoma Bank), anti- α -actinin (1:200; Abcam), anti- β -actin (1:2000; Cell Signaling Technology), and nuclei was visualized using appropriate species-specific Alexa Fluor 488- or Alexa Fluor 555-conjugated secondary antibodies and Hoechst 33342 (Thermo Fisher Scientific). Samples were then examined using an Olympus fluorescence microscope (Olympus Corporation). The relative ratio of Ki67-positive cells was calculated by dividing the number of Ki67-positive cells by the total number of nuclei, namely the total number of cells. The differentiation index was calculated by dividing the number of nuclei in myotubes (MyHC-positive elongated cells) by the total number of nuclei. The length of myotubes and the aspect ratio, which represents the ratio of width to length, were measured using ImageJ Fiji software (Schneider et al., 2012).

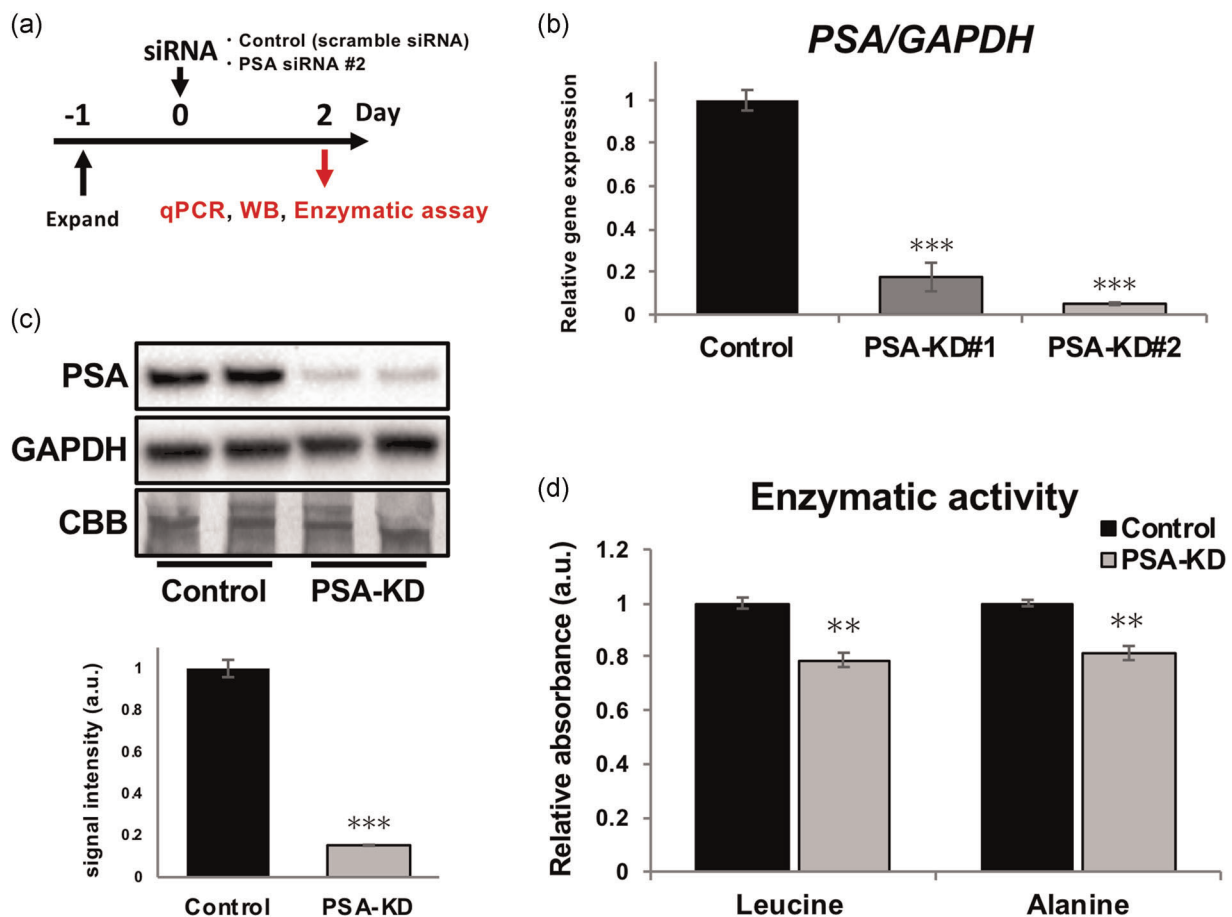


FIGURE 2 Loss of PSA expression suppresses enzymatic activity. (a) The time course of treatment and analysis in C2C12 myoblasts in which PSA was depleted using RNA interference (PSA-KD). (b) Real-time PCR analysis of PSA mRNA expression in C2C12 myoblasts in which PSA was depleted using RNA interference. PSA depletion led to a significant reduction of PSA mRNA levels in C2C12 myoblasts. Values are presented as the mean \pm SEM (Student's *t*-test: ****p* < .001 vs. control; *n* = 3 per group). (c) Immunoblotting of the protein levels of PSA in PSA-KD myoblasts. PSA protein expression was significantly decreased following PSA depletion in C2C12 myoblasts. Values are presented as the mean \pm SEM (Student's *t*-test: ****p* < .001 vs. control; *n* = 3 per group). (d) Measurement of the enzymatic activity of PSA on leucine and alanine substrates in PSA-KD myoblasts. PSA depletion resulted in significant inhibition of the aminopeptidase enzymatic activity on leucine and alanine substrates in C2C12 myoblasts. Values are presented as the mean \pm SEM (Student's *t*-test: ***p* < .01 vs. control; *n* = 3 per group). CBB, Coomassie brilliant blue; GAPDH, glyceraldehyde-3-phosphate dehydrogenase; mRNA, messenger RNA; PCR, polymerase chain reaction; PSA, puromycin-sensitive aminopeptidase

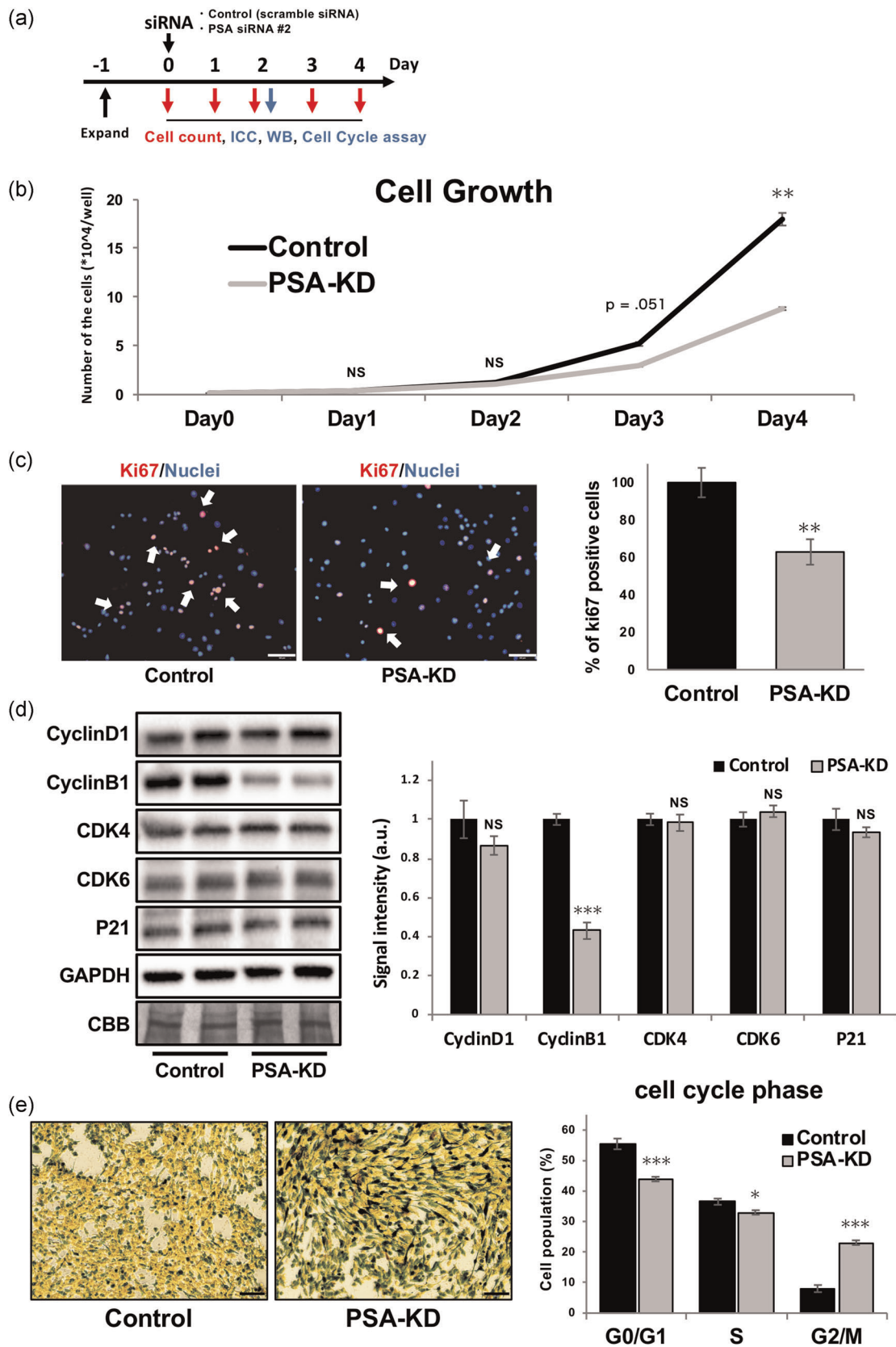


FIGURE 3 (See caption on next page)

2.6 | Aminopeptidase enzymatic activity

Cells were disrupted with RIPA buffer and transferred into 96-well plates. The lysate was combined with 1.6 mM leucine substrate (L-leucine-*p*-nitroaniline hydrochloride; FUJIFILM Wako Pure Chemical Corporation) and 0.7 mM alanine substrate (L-alanine-*p*-nitroaniline; Peptide Institute, Inc.) for 60 min at 37°C. Enzymatic activity was measured using a Multiskan Go Microplate Reader (Thermo Fisher Scientific) at an excitation and emission wavelength of 405 nm.

2.7 | Cell cycle assay

C2C12 myoblasts were cultured for 2 days after siRNA treatment in 24-well plates. The cell cycle status was measured using a Cell-Clock™ Cell Cycle Assay kit (Bicolor Life Science Assays). The treated cells were stained with the supplied redox dye (Cell-Clock Dye Reagent) for 1 h at 37°C, and images were captured using a fluorescence microscope. The percentage of cells in each phase was obtained from digitized photomicrographs using ImageJ Fiji software. G0/G1, S, and G2/M phase cells were stained yellow, green, and dark blue, respectively.

2.8 | Statistical analyses

Statistical analyses were performed using JMP Pro (SAS Institute) to determine significant differences from a two-tailed distribution using Student's *t*-test. $p < .05$ denoted statistical significance. Data are presented as the mean \pm SEM.

3 | RESULTS

3.1 | Expression of PSA in C2C12 myoblasts and myotubes

First, we examined the localization of PSA in C2C12 myoblasts and myotubes (Figure 1a). PSA expression was mainly localized in the cytoplasm in both C2C12 myoblasts (Figure 1b) and myotubes (Figure 1c). Following the induction of myogenic differentiation,

Myogenin and MyHC levels gradually increased, and MyoD levels gradually decreased, as reported previously. PSA expression was significantly increased at 2, 4, and 5 days after the induction of myogenic differentiation compared with expression levels before induction of myogenic differentiation (Figure 1d).

3.2 | Investigation of enzymatic activity in PSA-KD myoblasts

To deplete PSA gene and protein expression, the PSA gene was knocked down in C2C12 myoblasts using three siRNAs (Figures 2a and S1a). siRNA#2 reduced PSA gene expression by more than 95% in myoblasts compared with the effect of scrambled siRNA (control; Figures 2B and S1b). PSA protein levels were significantly reduced in cells transfected with siRNA#2 (Figure 2c). For the following experiments, we decide to use siRNA#2 for PSA depletion. The PSA enzymatic activities for leucine and alanine substrates were suppressed in PSA-KD myoblasts (Figure 2d).

3.3 | PSA depletion leads to impaired cell cycle progression

We investigated cell proliferation capacity in PSA-KD myoblasts by cell count, immunocytochemistry, Western blot, and cell cycle assays (Figure 3a). The number of cells was significantly decreased 4 days after PSA depletion (Figures 3B and S1c). Additionally, the number of Ki67-positive cells was significantly decreased by PSA depletion (Figure 3c). Next, we examined the expression of cell cycle-related proteins in PSA-KD myoblasts. Cyclin D1 and CDK4/6 complex are required for the progression of the G1 phase of the cell cycle, and p21 is known to inhibit the activity of the complex. We found that the levels of these proteins were not changed in PSA-KD myoblasts (Figures 3D and S1d). The level of cyclin B1, essential for mitosis (Strauss et al., 2018), was significantly decreased in PSA-KD myoblasts (Figures 3D and S1d). Consequently, cell cycle analysis of PSA-KD myoblasts revealed a significantly reduced G0/G1 and S phase subpopulations as compared with that in the control cells, and the accumulation of G2/M phase population in PSA-KD as compared to the control cells (Figures 3E and S1e).

FIGURE 3 Genetic loss of PSA impairs cell cycle progression. (a) The time course of treatment and analysis in C2C12 myoblasts in which PSA was depleted using RNA interference (PSA-KD). (b) Evaluation of cell growth 0, 1, 2, 3, and 4 days after PSA depletion in C2C12 myoblasts. Cell growth was significantly decreased in PSA-KD myoblasts at 4 days after PSA depletion. Values are presented as the mean \pm SEM (Student's *t*-test: NS, not significant, $**p < .01$ vs. control; $n = 3$ per group). (c) Immunocytochemistry for Ki67 (red) and nuclei (blue) in PSA-KD myoblasts. The relative ratio of Ki67-positive cells was significantly reduced in PSA-KD myoblasts. Scale bar = 100 μ m. Values are presented as the mean \pm SEM (Student's *t*-test: $**p < .01$ vs. control; $n = 6$ per group). (d) Immunoblotting of the protein levels of cyclin D1, cyclin B1, CDK4, CDK6, p21, and GAPDH in PSA-KD myoblasts. PSA depletion resulted in a significant reduction of cyclin B1 levels, whereas cyclin D1, CDK4, CDK6, and P21 levels were unchanged. Values are presented as the mean \pm SEM (Student's *t*-test: NS, not significant, $**p < .001$ vs. control; $n = 3$ per group). (e) Cell cycle analysis in PSA-KD myoblasts. The populations of cells in the G0/G1 and S phase were significantly reduced in PSA-KD myoblasts, whereas the G2/M phase population was significantly increased. Scale bar = 100 μ m. Values are presented as the mean \pm SEM (Student's *t*-test: $*p < .05$, $***p < .001$ vs. control; $n = 3$ per group). CBB, Coomassie brilliant blue; CDK, cyclin-dependent kinase; GAPDH, glyceraldehyde-3-phosphate dehydrogenase; PSA, puromycin-sensitive aminopeptidase

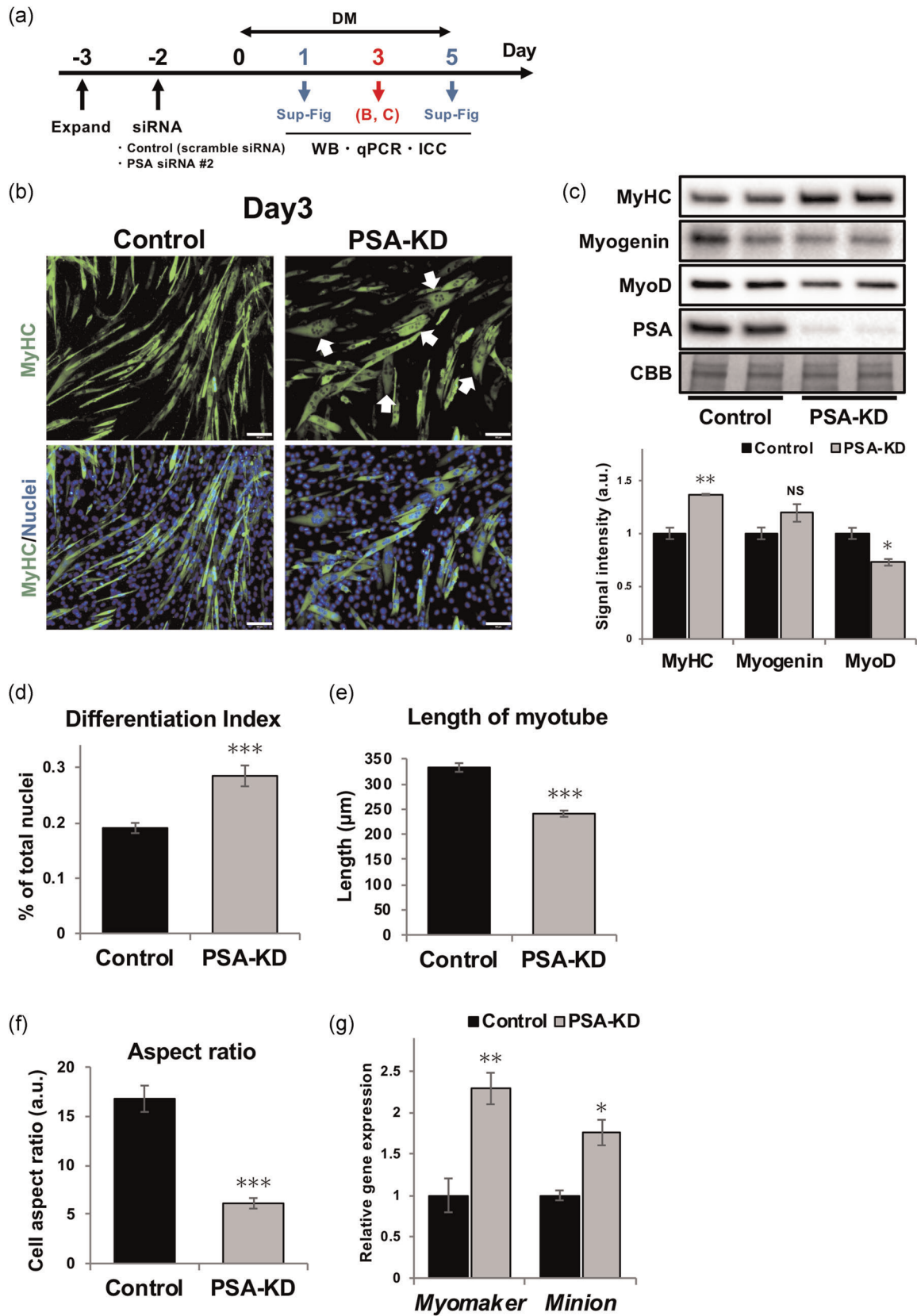


FIGURE 4 (See caption on next page)

3.4 | PSA-KD myoblasts exhibit irregular myogenic differentiation

To reveal the potential role of PSA in C2C12 myoblast differentiation, myogenic differentiation was induced in PSA-KD myoblasts, and their differentiation was assessed by immunocytochemistry, Western blot analysis, and qPCR (Figure 4a). MyHC expression was increased in PSA-KD myotubes as well as control myotubes, following the induction of myotube formation; however, PSA-KD myotubes displayed apparent morphological abnormalities after 3 and 5 days of myogenic differentiation (Figure 4B, white arrows; Figures S2a,c and S3a). After 1 day of myogenic differentiation, MyHC expression was weaker in PSA-KD myoblasts relative to expression in control myoblasts, whereas MyoD and Myogenin levels were similar in both conditions (Figure S2b). After 3 days of myogenic differentiation, the increase in MyHC expression levels was markedly enhanced in PSA-KD myoblasts compared with expression in control myoblasts. On the other hand, the level of MyoD expression was significantly lower in PSA-KD myoblasts relative to expression in control myoblasts. However, Myogenin expression levels did not differ between the two conditions (Figure 4c). Furthermore, the differentiation index, representing the number of nuclei per myotube, was significantly increased in PSA-KD myoblasts (Figures 4D and S3b). Additionally, the length of the myotubes was significantly shorter for PSA-KD myotubes than for control myotubes (Figures 4E and S3b). Consequently, the aspect ratio was significantly decreased in PSA-KD myotubes (Figures 4F and S3b). After 5 days of differentiation, the level of Myogenin expression was reduced in PSA-KD myoblasts, whereas MyHC and MyoD expression levels did not differ between PSA-KD and control myoblasts (Figure S2d). In addition, the differentiation index was significantly increased in PSA-KD myoblasts (Figures S2e and S3c). Additionally, the length of the myotubes was significantly shorter for PSA-KD myotubes than for control myotubes (Figures S2F and S3C). Consequently, the aspect ratio was significantly decreased in PSA-KD myotubes (Figures S2G and S3C).

The fusion of myoblasts is essential for the formation of multinucleated myotubes. Myomaker and Minion are muscle-specific

fusion proteins responsible for myoblast plasma membrane fusion (Bi et al., 2017; Zhang et al., 2017). After 1 day of differentiation, these mRNA levels were no different in the levels of *Myomaker* and *Minion* expression in PSA-KD myoblasts and control cells (Figure S4A). Expectedly, after 3 days of myogenic differentiation, the level of *Myomaker* and *Minion* mRNA expression was significantly higher in PSA-KD myotubes (Figure 4g). Furthermore, after 5 days of myogenic differentiation, the level of *Myomaker* mRNA expression remained significantly larger, but there was no statistically significant difference in the level of *Minion* mRNA expression (Figure S4b).

3.5 | Cell polarity disappears in the early phase of myogenic differentiation of PSA-KD myoblasts

Reorganization of the cytoskeleton is essential for myoblast fusion and myotube formation (Guerin & Kramer, 2009). Therefore, to identify the structural organization of the cytoskeleton, we performed immunocytochemistry in PSA-KD myotubes (Figure 5a). In normal myotubes, β -actin and α -actinin were elongated, with the direction of myotube formation exhibiting a linear strain (Figures 5B and S5). However, in PSA-KD myotubes, β -actin and α -actinin linear structures were not identified (Figures 5B and S5). Because cell polarity is involved in cytoskeleton formation, we examined the expression of CDC42, a key regulator of cell polarity and a Rho family GTPase (Etienne-Manneville, 2004), during myogenic differentiation in PSA-KD myoblasts. Before the induction of differentiation, there was no difference in CDC42 levels between control and PSA-KD myoblasts (Figure 5c). Interestingly, however, after 1 and 3 days of myogenic differentiation, there was a clear and significant reduction in CDC42 expression levels in PSA-KD myoblasts (Figure 5c).

3.6 | CDC42 depletion leads to apparent morphological abnormalities in myotubes

To examine whether depletion of CDC42 affects myotube formation was assessed by immunocytochemistry and Western blot analysis

FIGURE 4 Loss of PSA expression in myoblasts results in irregular myogenic differentiation. (a) The time course of treatment and analysis in C2C12 myotubes in which PSA was depleted using RNA interference (PSA-KD). (b) Immunocytochemistry for myosin heavy chain (MyHC, green) and nuclei (blue) in PSA-KD myotubes at 3 days after myogenic differentiation. PSA depletion led to abnormalities of myotube morphology (white arrows) after 3 days of myogenic differentiation. Scale bar = 100 μ m. (c) Immunoblotting of the protein levels of MyHC, myogenin, MyoD, and PSA 3 days after the induction of myogenic differentiation in PSA-KD myoblasts. MyHC expression increased significantly in PSA-KD myoblasts, while MyoD and PSA levels were significantly reduced and myogenin levels were not changed. Values are presented as the mean \pm SEM (Student's *t*-test: NS, not significant, **p* < .05, ***p* < .01 vs. control; *n* = 3 per group). (d) The differentiation index was significantly reduced in PSA-KD myotubes after 3 days of myogenic differentiation. Values are presented as the mean \pm SEM (Student's *t*-test: ****p* < .001 vs. control; *n* = 5 per group). (e,f) The length and aspect ratio of myotubes were significantly reduced in PSA-KD myotubes after 3 days of myogenic differentiation as measured using ImageJ software. Values are presented as the mean \pm SEM (Student's *t*-test: ****p* < .001 vs. control; *n* = 5 per group, *n* = 100 number of myotube in each sample). (g) Quantitative real-time PCR analysis of the mRNA levels of *Myomaker* and *Minion* 3 days after the induction of myogenic differentiation in PSA-KD myoblasts. *Myomaker* and *Minion* mRNA levels were significantly increased. Values are presented as the mean \pm SEM (Student's *t*-test: NS, not significant, **p* < .05, ***p* < .01 vs. control; *n* = 3 per group). CBB, Coomassie brilliant blue; MyHC, myosin heavy chain; MyoD, myoblast determination protein 1; PSA, puromycin-sensitive aminopeptidase

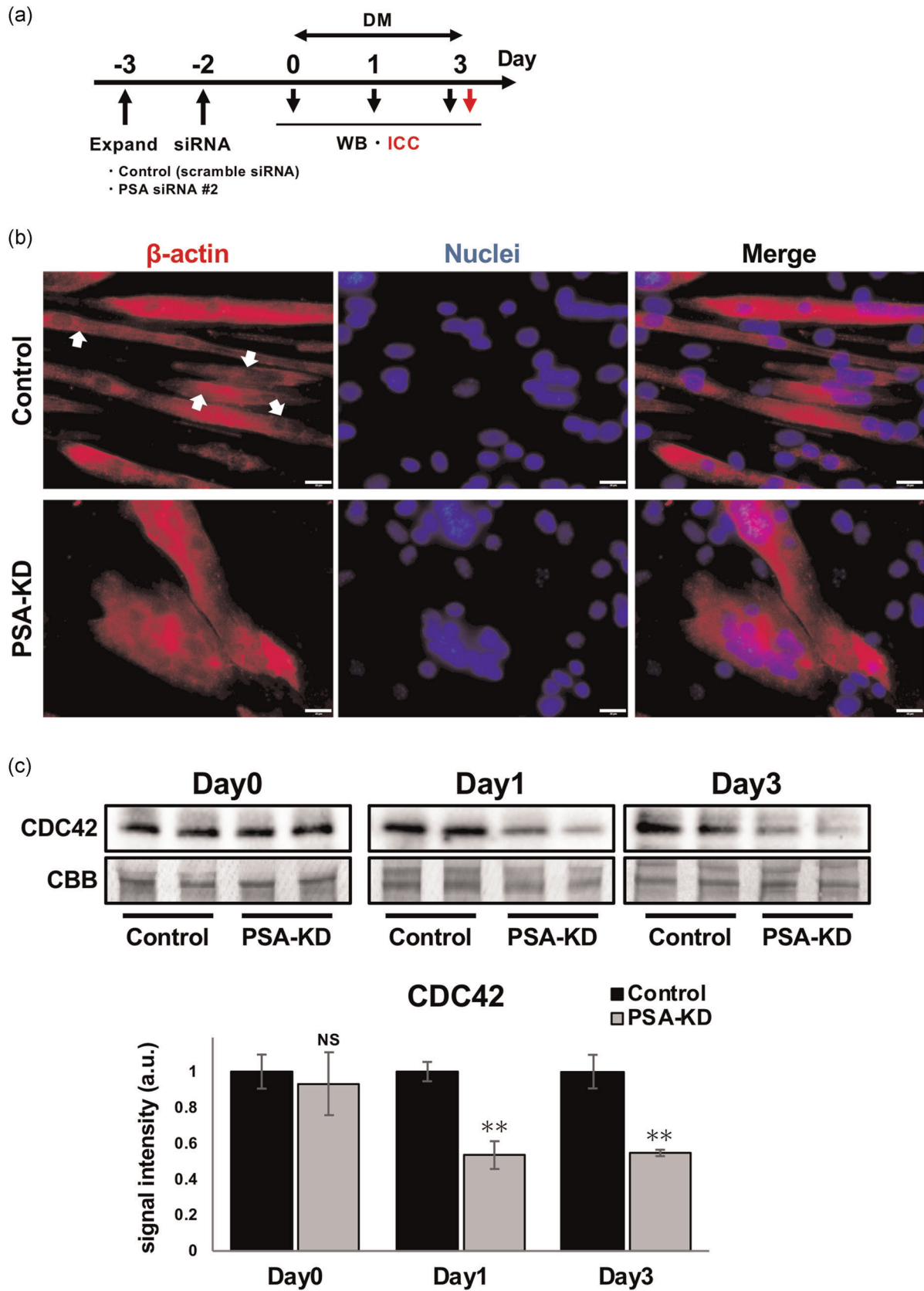


FIGURE 5 (See caption on next page)

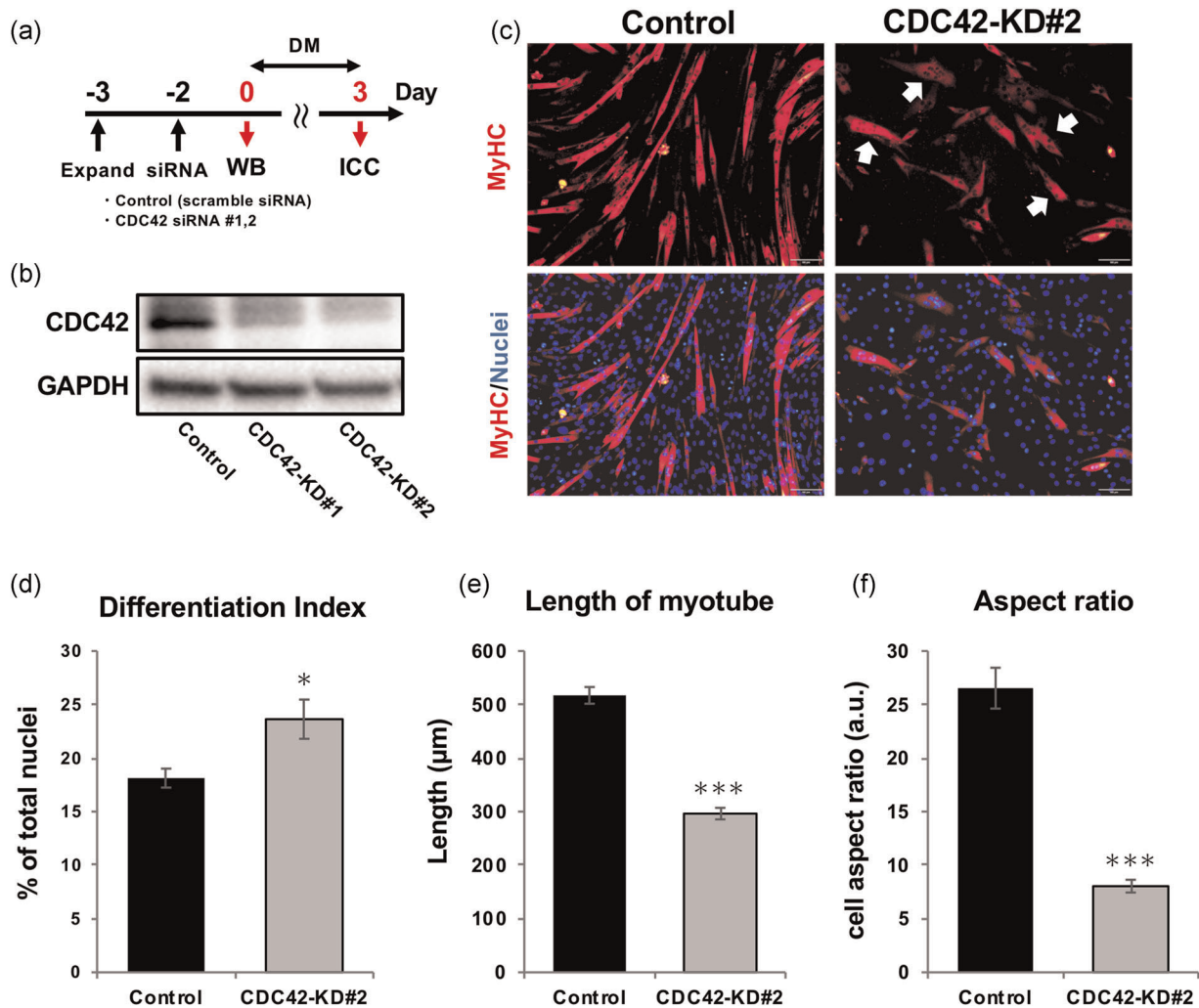


FIGURE 6 CDC42 depletion leads to apparent morphological abnormalities in myotubes. (a) The time course of treatment and analysis in C2C12 myotubes in which CDC42 was depleted using RNA interference#1, #2 (CDC42-KD). (b) Immunoblotting of the protein levels of CDC42 in CDC42-KD myoblasts. CDC42 protein expression was markedly decreased following CDC42 depletion in C2C12 myoblasts. (c) Immunocytochemistry for myosin heavy chain (MyHC, red) and nuclei (blue) in CDC42-KD#2 myotubes at 3 days after myogenic differentiation. CDC42 depletion led to abnormalities in myotube morphology (white arrows) after 3 days of myogenic differentiation. Scale bar = 100 μm. (d) The differentiation index was significantly reduced in CDC42-KD#2 myotubes after 3 days of myogenic differentiation. Values are presented as the mean ± SEM (Student's *t*-test: **p* < .05 vs. control; *n* = 6 per group). (e,f) The length and aspect ratio of myotubes were significantly reduced in CDC42-KD#2 myotubes after 3 days of myogenic differentiation (as measured using ImageJ software). Values are presented as the mean ± SEM (Student's *t*-test: ****p* < .001 vs. control; *n* = 6 per group; *n* = 100 myotubes in each sample). GAPDH, glyceraldehyde-3-phosphate dehydrogenase; MyHC, myosin heavy chain

(Figures 6A and S6A). To inhibit CDC42 protein expression, the CDC42 gene was knocked down in C2C12 myoblasts using two siRNAs. CDC42 protein levels were markedly reduced in cells transfected with siRNA#2 (Figure 6c). MyHC expression was increased in

CDC42-KD#2 myotubes as well as the control myotubes following the induction of myotube formation, but CDC42-KD myotubes displayed apparent morphological abnormalities after 3 and 5 days of myogenic differentiation similar to PSA-KD myotubes (Figure 6C, white arrows;

FIGURE 5 Depletion of PSA in myotubes impaired cytoskeleton formation and cell polarity. (a) The time course of treatment and analysis in C2C12 myotubes in which PSA was depleted using RNA interference (PSA-KD). (b) Immunocytochemistry for β-actin (red) and nuclei (blue) in PSA-KD myotubes. In normal myotubes, β-actin was elongated along with the direction of myotube formation. PSA depletion resulted in an abnormal β-actin structure. Scale bar = 20 μm. (c) Immunoblotting of CDC42 protein levels 0, 1, and 3 days after the induction of myogenic differentiation in PSA-KD myoblasts. CDC42 expression was unchanged in PSA-KD myoblasts before myogenic induction. After 1 and 3 days of myogenic differentiation, CDC42 expression was significantly decreased. Values are presented as the mean ± SEM (Student's *t*-test: NS, not significant, ***p* < .01 vs. control; *n* = 3 per group). CBB, Coomassie brilliant blue; PSA, puromycin-sensitive aminopeptidase

Figure S6b). After 3 and 5 days of differentiation, the differentiation index was significantly increased in CDC42-KD myoblasts (Figures 6D and S6C). Interestingly, however, CDC42-KD myotubes were significantly shorter in length than control myotubes (Figures 6E and S6C). Consequently, the aspect ratio was significantly decreased in PSA-KD myotubes (Figures 6F and S6C).

4 | DISCUSSION

In this study, we revealed that PSA was mainly localized in the cytoplasm in myoblasts, and the protein was associated with cell cycle progression. Specifically, PSA depletion resulted in significant reductions in the levels of cyclin B1, involved in the cell cycle progression from G2 to M phase (Dienemann & Sprenger, 2004; Gavet & Pines, 2010), but not the levels of cyclin D1 and CDK4/6 complex, essential for cell cycle progression from G1 to S phase (Albrecht & Hansen, 1999; Du et al., 2013). A previous study reported that PSA localized to the cytoplasm (Constam et al., 1995). In addition, the treatment with puromycin, which inhibits PSA, arrested the cell cycle, leading to the accumulation of cells in the G2/M phase (Jans et al., 2001; Yuan et al., 2004). These results are in line with the result of the present study. It was previously reported that ubiquitin-proteasome-dependent protein degradation regulates the cell cycle and mediates the timely and precise expression of key cell cycle proteins, such as cyclins and CDKs (Bassermann et al., 2014; Tu et al., 2012). Our results further support these observations and suggest that the cell cycle regulation by proteasome-dependent protein degradation is mediated by the downstream activity of PSA.

We previously reported that proteasome dysfunction in satellite cells induced apoptosis, resulting in the loss of the cells (Kitajima et al., 2018). The inhibition of intracellular aminopeptidase by Bes-ME and depletion of PSA, however, did not induce cell death. This apparent discrepancy may be because proteasome dysfunction-induced apoptosis is a consequence of impaired degradation of ubiquitinated p53 (Maki et al., 1996). The proteasome dysfunction in our previous study differs from the PSA depletion in the present study or chemical inhibition by Bes-ME in which the proteasome function itself remains intact. Therefore, PSA activity downstream of proteasomal proteolysis is not involved in cell loss due to apoptosis in proteasomal-defective satellite cells.

In this study, differentiated PSA-KD myotubes exhibited a spherical structure, an abnormal phenotype in myogenic differentiation. Recent studies have identified intracellular microprotein, Myomaker and Minion (also called Myomixer or Myomerger), to be essential for myoblast fusion (Bi et al., 2017; Millay et al., 2013; Quinn et al., 2017; Zhang et al., 2017). The expression of Myomaker and Minion, which have definitive roles in the plasma membrane fusion of myoblasts, is increased during myogenic differentiation. Interestingly, overexpression of both Myomaker and Minion in myoblasts using vectors resulted in the formation of spherical myotubes (Bi et al., 2017), similar to PSA-KD myotubes in this study. Considering the increased expression of *Myomaker* and

Minion mRNA in PSA-KD myoblasts during myogenic differentiation, it is possible that the excessive fusion of myoblasts due to enhanced expression of these proteins was responsible for the spherical myotubes in this study. This is the first report in which the involvement of aminopeptidases was demonstrated in the regulation of myoblast fusion.

Cell polarity is important in morphogenesis during tissue development and adult tissue regeneration. The absence of cell polarization can lead to tissue disorganization (Martin-Belmonte & Perez-Moreno, 2011). In myoblasts, cell polarity is essential for fusion and differentiation (Cadot et al., 2012). CDC42 is one of the major regulators of cytoskeletal and cellular polarization (Etienne-Manneville, 2004). In the present study, induction of myogenic differentiation on CDC42-KD myoblasts resulted in myotubes with a spherical structure, similar to PSA-KD myotubes. Therefore, the spherical structure of PSA-KD myotubes may be attributable to abnormal cell polarity caused by CDC42 downregulation in the early phase of myogenic differentiation.

In conclusion, loss of PSA in myoblasts exhibited impaired cell cycle progression, abnormal myotube formation, and a lack of cell polarization. These data suggest that PSA contributes to the proliferation and differentiation of myoblasts.

ACKNOWLEDGMENTS

This study was supported by JSPS KAKENHI Grant Numbers 18H04080 and 20K19478.

CONFLICT OF INTERESTS

The authors declare that there are no conflict of interests.

AUTHOR CONTRIBUTIONS

Shion Osana designed the experiments, performed the experiments, interpreted the data, assembled the input data, and wrote the manuscript. Yasuo Kitajima, Naoki Suzuki, and Aki Nunomiya interpreted the data. Hiroaki Takada, Takahiro Kubota, and Kazutaka Murayama performed the experiments. Ryoichi Nagatomi interpreted the data, assembled the input data, and wrote the manuscript. All authors discussed the results and implications and commented on the manuscript.

DATA AVAILABILITY STATEMENT

All relevant data are within the article. The data that support the findings of this study are available from the corresponding author upon reasonable request.

ORCID

Shion Osana  <http://orcid.org/0000-0001-8998-252X>

Ryoichi Nagatomi  <https://orcid.org/0000-0003-3038-7202>

REFERENCES

- Albrecht, J. H., & Hansen, L. K. (1999). Cyclin D1 promotes mitogen-independent cell cycle progression in hepatocytes. *Cell Growth & Differentiation*, 10(6), 397–404.

- Bassermann, F., Eichner, R., & Pagano, M. (2014). The ubiquitin proteasome system - implications for cell cycle control and the targeted treatment of cancer. *Biochimica et Biophysica Acta*, 1843(1), 150–162. <https://doi.org/10.1016/j.bbamcr.2013.02.028>
- Bi, P., Ramirez-Martinez, A., Li, H., Cannavino, J., McAnally, J. R., Shelton, J. M., Sánchez-Ortiz, E., Bassel-Duby, R., & Olson, E. N. (2017). Control of muscle formation by the fusogenic micropeptide myomixer. *Science*, 356(6335), 323–327. <https://doi.org/10.1126/science.aam9361>
- Botbol, V., & Scornik, O. A. (1983). Peptide intermediates in the degradation of cellular proteins. Bestatin permits their accumulation in mouse liver in vivo. *Journal of Biological Chemistry*, 258(3), 1942–1949.
- Botbol, V., & Scornik, O. A. (1997). Measurement of muscle protein degradation in live mice by accumulation of bestatin-induced peptides. *American Journal of Physiology*, 273(6), E1149–E1157. <https://doi.org/10.1152/ajpendo.1997.273.6.E1149>
- Brack, A. S., & Rando, T. A. (2012). Tissue-specific stem cells: Lessons from the skeletal muscle satellite cell. *Cell Stem Cell*, 10(5), 504–514. <https://doi.org/10.1016/j.stem.2012.04.001>
- Cadot, B., Gache, V., Vasyutina, E., Falcone, S., Birchmeier, C., & Gomes, E. R. (2012). Nuclear movement during myotube formation is microtubule and dynein dependent and is regulated by Cdc42, Par6 and Par3. *EMBO Reports*, 13(8), 741–749. <https://doi.org/10.1038/embor.2012.89>
- Collins, G. A., & Goldberg, A. L. (2017). The logic of the 26S proteasome. *Cell*, 169(5), 792–806. <https://doi.org/10.1016/j.cell.2017.04.023>
- Constam, D. B., Tobler, A. R., Rensing-Ehl, A., Kemler, I., Hersh, L. B., & Fontana, A. (1995). Puromycin-sensitive aminopeptidase. Sequence analysis, expression, and functional characterization. *Journal of Biological Chemistry*, 270(45), 26931–26939. <https://doi.org/10.1074/jbc.270.45.26931>
- Dienemann, A., & Sprenger, F. (2004). Requirements of cyclin a for mitosis are independent of its subcellular localization. *Current Biology*, 14(12), 1117–1123. <https://doi.org/10.1016/j.cub.2004.06.024>
- Du, Z., Tong, X., & Ye, X. (2013). Cyclin D1 promotes cell cycle progression through enhancing NDR1/2 kinase activity independent of cyclin-dependent kinase 4. *Journal of Biological Chemistry*, 288(37), 26678–26687. <https://doi.org/10.1074/jbc.M113.466433>
- Etienne-Manneville, S. (2004). Cdc42—The centre of polarity. *Journal of Cell Science*, 117(Pt 8), 1291–1300. <https://doi.org/10.1242/jcs.01115>
- Gavet, O., & Pines, J. (2010). Progressive activation of CyclinB1-Cdk1 coordinates entry to mitosis. *Developmental Cell*, 18(4), 533–543. <https://doi.org/10.1016/j.devcel.2010.02.013>
- Goldberg, A. L. (2003). Protein degradation and protection against misfolded or damaged proteins. *Nature*, 426(6968), 895–899. <https://doi.org/10.1038/nature02263>
- Guerin, C. M., & Kramer, S. G. (2009). Cytoskeletal remodeling during myotube assembly and guidance: Coordinating the actin and microtubule networks. *Communicative and Integrative Biology*, 2(5), 452–457. <https://doi.org/10.4161/cib.2.5.9158>
- Hershko, A., & Ciechanover, A. (1992). The ubiquitin system for protein degradation. *The Annual Review of Biochemistry*, 61, 761–807. <https://doi.org/10.1146/annurev.bi.61.070192.003553>
- Hershko, A., & Ciechanover, A. (1998). The ubiquitin system. *The Annual Review of Biochemistry*, 67, 425–479. <https://doi.org/10.1146/annurev.biochem.67.1.425>
- Janss, A. J., Maity, A., Tang, C. B., Muschel, R. J., McKenna, W. G., Sutton, L., & Phillips, P. C. (2001). Decreased cyclin B1 expression contributes to G2 delay in human brain tumor cells after treatment with camptothecin. *Neuro-Oncology*, 3(1), 11–21. <https://doi.org/10.1093/neuonc/3.1.11>
- Kitajima, Y., Suzuki, N., Nunomiya, A., Osana, S., Yoshioka, K., Tashiro, Y., Takahashi, R., Ono, Y., Aoki, M., & Nagatomi, R. (2018). The ubiquitin-proteasome system is indispensable for the maintenance of muscle stem cells. *Stem Cell Reports*, 11(6), 1523–1538. <https://doi.org/10.1016/j.stemcr.2018.10.009>
- Kitajima, Y., Tashiro, Y., Suzuki, N., Warita, H., Kato, M., Tateyama, M., Ando, R., Izumi, R., Yamazaki, M., Abe, M., Sakimura, K., Ito, H., Urushitani, M., Nagatomi, R., Takahashi, R., & Aoki, M. (2014). Proteasome dysfunction induces muscle growth defects and protein aggregation. *Journal of Cell Science*, 127(Pt 24), 5204–5217. <https://doi.org/10.1242/jcs.150961>
- Maki, C. G., Huibregtse, J. M., & Howley, P. M. (1996). In vivo ubiquitination and proteasome-mediated degradation of p53(1). *Cancer Research*, 56(11), 2649–2654.
- Martin-Belmonte, F., & Perez-Moreno, M. (2011). Epithelial cell polarity, stem cells and cancer. *Nature Reviews Cancer*, 12(1), 23–38. <https://doi.org/10.1038/nrc3169>
- Millay, D. P., O'Rourke, J. R., Sutherland, L. B., Bezprozvannaya, S., Shelton, J. M., Bassel-Duby, R., & Olson, E. N. (2013). Myomaker is a membrane activator of myoblast fusion and muscle formation. *Nature*, 499(7458), 301–305. <https://doi.org/10.1038/nature12343>
- Morgan, J. E., & Partridge, T. A. (2003). Muscle satellite cells. *The International Journal of Biochemistry & Cell Biology*, 35(8), 1151–1156. [https://doi.org/10.1016/s1357-2725\(03\)00042-6](https://doi.org/10.1016/s1357-2725(03)00042-6)
- Mucha, A., Drag, M., Dalton, J. P., & Kafarski, P. (2010). Metallo-aminopeptidase inhibitors. *Biochimie*, 92(11), 1509–1529. <https://doi.org/10.1016/j.biochi.2010.04.026>
- Osana, S., Kitajima, Y., Suzuki, N., Xu, Y., Murayama, K., & Nagatomi, R. (2020). siRNA knockdown of alanine aminopeptidase impairs myoblast proliferation and differentiation. *Experimental Cell Research*, 397(1), 112337. <https://doi.org/10.1016/j.yexcr.2020.112337>
- Osana, S., Murayama, K., & Nagatomi, R. (2020). The impact of intracellular aminopeptidase on C2C12 myoblast proliferation and differentiation. *Biochemical and Biophysical Research Communications*, 524(3), 608–613. <https://doi.org/10.1016/j.bbrc.2020.01.115>
- Quinn, M. E., Goh, Q., Kurosaka, M., Gamage, D. G., Petrany, M. J., Prasad, V., & Millay, D. P. (2017). Myomergin induces fusion of non-fusogenic cells and is required for skeletal muscle development. *Nature Communications*, 8, 15665. <https://doi.org/10.1038/ncomms15665>
- Saric, T., Graef, C. I., & Goldberg, A. L. (2004). Pathway for degradation of peptides generated by proteasomes: A key role for thimet oligopeptidase and other metallopeptidases. *Journal of Biological Chemistry*, 279(45), 46723–46732. <https://doi.org/10.1074/jbc.M406537200>
- Schneider, C. A., Rasband, W. S., & Eliceiri, K. W. (2012). NIH Image to ImageJ: 25 years of image analysis. *Nature Methods*, 9(7), 671–675. <https://doi.org/10.1038/nmeth.2089>
- Sengupta, S., Horowitz, P. M., Karsten, S. L., Jackson, G. R., Geschwind, D. H., Fu, Y., Berry, R. W., & Binder, L. I. (2006). Degradation of tau protein by puromycin-sensitive aminopeptidase in vitro. *Biochemistry*, 45(50), 15111–15119. <https://doi.org/10.1021/bi061830d>
- Strauss, B., Harrison, A., Coelho, P. A., Yata, K., Zernicka-Goetz, M., & Pines, J. (2018). Cyclin B1 is essential for mitosis in mouse embryos, and its nuclear export sets the time for mitosis. *Journal of Cell Biology*, 217(1), 179–193. <https://doi.org/10.1083/jcb.201612147>
- Tu, Y., Chen, C., Pan, J., Xu, J., Zhou, Z. G., & Wang, C. Y. (2012). The ubiquitin proteasome pathway (UPP) in the regulation of cell cycle control and DNA damage repair and its implication in tumorigenesis. *International Journal of Clinical and Experimental Pathology*, 5(8), 726–738.
- Yin, H., Price, F., & Rudnicki, M. A. (2013). Satellite cells and the muscle stem cell niche. *Physiological Reviews*, 93(1), 23–67. <https://doi.org/10.1152/physrev.00043.2011>

- Yuan, J., Yan, R., Kramer, A., Eckerdt, F., Roller, M., Kaufmann, M., & Strebhardt, K. (2004). Cyclin B1 depletion inhibits proliferation and induces apoptosis in human tumor cells. *Oncogene*, 23(34), 5843–5852. <https://doi.org/10.1038/sj.onc.1207757>
- Zammit, P. S. (2017). Function of the myogenic regulatory factors Myf5, MyoD, Myogenin and MRF4 in skeletal muscle, satellite cells and regenerative myogenesis. *Seminars in Cell and Developmental Biology*, 72, 19–32. <https://doi.org/10.1016/j.semcdb.2017.11.011>
- Zhang, Q., Vashisht, A. A., O'Rourke, J., Corbel, S. Y., Moran, R., Romero, A., Miraglia, L., Zhang, J., Durrant, E., Schmedt, C., Sampath, S. C., & Sampath, S. C. (2017). The microprotein Minion controls cell fusion and muscle formation. *Nature Communications*, 8, 15664. <https://doi.org/10.1038/ncomms15664>

SUPPORTING INFORMATION

Additional Supporting Information may be found online in the supporting information tab for this article.

How to cite this article: Osana S, Kitajima Y, Suzuki N, et al. Puromycin-sensitive aminopeptidase is required for C2C12 myoblast proliferation and differentiation. *J Cell Physiol.* 2021;236:5293–5305. <https://doi.org/10.1002/jcp.30237>